PERGAMON

International Journal of Heat and Mass Transfer 42 (1999) 3469–3480

International Journal of HEAT and MASS TRANSFER

The influence of soot loading on weighted sum of grey gases solutions to the radiative transfer equation across mixtures of gases and soot

N.W. Bressloff*

Department of Aeronautics and Astronautics, Computational and Engineering and Design Centre, University of Southampton, Highfield, Southampton SO17 1BJ, UK

Received 20 November 1997; received in revised form 9 December 1998

Abstract

Different approaches to employing weighted sum of grey gases data in line of sight solutions to the radiative transfer equation (RTE) are compared for mixtures of combustion gases and soot. Responses to variations in soot loading are analysed across configurations comprising uniform and non-uniform properties and compositions. Relative to a differential banded transmissivity solution, a weighted sum of grey gases (WSGG) solution, which solves the RTE for each grey gas component, yields greater accuracy than a total property (TP) solution. The latter evaluates radiative properties on a cell-by-cell basis for application in a single equation. However, accuracy of the TP solution is shown to improve with increasing soot loading.

1. Introduction

The transfer of energy by thermal radiation is a highly complex multi-dimensional phenomenon. A detailed computational solution of the equation describing this process of energy transfer—the radiative transfer equation (RTE)—is prohibitively expensive. Thus, when radiative energy exchange is incorporated into computational fluid dynamics (CFD) simulations of combusting media [1], approximate solutions of the RTE must be used, and available levels of computing power primarily determine the degree of approximation. This paper presents a comparison between two methods for employing weighted sum of grey gases data to solve the RTE within the discrete transfer radiation model (DTRM) [2]. The first involves a weighted sum of grey gases (WSGG) solution to the RTE [3] which models the non-grey characteristics of emission and absorption by solving separate transfer equations for each grey gas component. In contrast, a more approximate method which does not take account of the non-grey behaviour of thermal radiation, the total property (TP) solution, solves one equation along each line of sight with radiative properties encapsulated in a single (total) emissivity for each elemental path.

A number of methods for solving the RTE were reviewed in [4]. Luminous and non-luminous radiation were considered across both homogeneous and non-homogeneous paths. However, this treatment was primarily directed at the prediction of total flame emissivity with little consideration of coupled flow-radiation calculations. A more extensive review of radiation heat transfer was provided in [5] which included a survey of global radiation models. Nonetheless, there were no references to detailed analyses of modelling techniques

* Tel.: +44 01703 595 076; fax: +44 01703 593 058.
E-mail address: nwb@soton.ac.uk (N.W. Bressloff)

0017-9310/99/$ - see front matter
PII: S0017-9310(99)00031-9

Nomenclature

a	grey gas polynomial weighting coefficient
i	radiative intensity, kW/m^2/sr
i_ν	radiative intensity, kW/m^2/sr/cm
k	absorption coefficient, m^{-1}
p	partial pressure, atm
s, s', s''	distance, m
T	temperature, K
w	weighting of radiative intensity, sr.

Greek symbols

ϵ	emissivity
σ	Stefan–Boltzmann constant, kW/m^2/K^4
τ	transmissivity
Φ	soot volume fraction.

Subscripts

b	black body quantities
c	carbon dioxide
h	water
j	spectral band or grey gas component
m	ray descriptor
n, r, r'	computational grid cell
N	final cell in path
p	particulate
s	source temperature
ν	wave number
0	origin of path.

Superscripts

c	correlated solution
T	total property.

within a particular radiation model. Such analysis has been performed for the discrete ordinates [6,7], the Monte Carlo [8] and the discrete transfer [9–12] radiation models; and the results presented here complement this body of work.

The DTRM has been particularly widely used for modelling various combustion media [13], largely due to the fact that it does not obscure the physical nature of thermal radiation by its mathematical treatment. Generally, it has been applied in coupled fluid dynamics heat transfer calculations by employing a total property (TP) solution [14,15] as described below. Alternatively, data from flow field simulations have been post-processed [10,16]. Reference [10] is especially pertinent in the present context since the flow field solution obtained using a grey DTRM calculation was then used to compare a narrow band and a weighted sum of grey gases model predictions of surface and volumetric flux. Good agreement was observed for the case of a hot medium surrounded by relatively cold walls. More recently, Bressloff et al. [11,12] presented detailed analyses of various algorithms in their development of the differential total absorptivity (DTA) solution to the radiative transfer equation for application in the DTRM. Although superior accuracy of the DTA solution was demonstrated relative to the WSGG solution, the accompanying order of magnitude cost penalty of the former, suggested that the WSGG solution may offer the best compromise between accuracy and cost with current levels of computing power. However, this assertion requires knowledge of the relative merits of the WSGG solution and the more approximate TP solution.

Attention is initially focused upon line-of-sight solutions to the RTE which facilitates an assessment of individual algorithms without obscuring their performance by features of the DTRM. A significant difference in performance is identified between the WSGG and

TP solutions through an analysis of the radiative intensity variation across uniform gas–soot mixtures comprising varying concentrations of soot. The solutions are then compared across non-isothermal, non-homogeneous mixtures again possessing different levels of soot loading. Finally, the same non-uniform mixture profiles are adopted in an assessment of the solutions as applied in the DTRM. In all cases, only emitting–absorbing media are considered comprising CO_2, H_2O and soot. The neglect of scattering is justifiable for combustion environments where soot particles are small relative to the wavelength range of thermal radiation [13]. Grosshandler's computer code, RADCAL [17] employing the statistical narrow band model [18] is used here as the benchmark for comparing the more approximate methods.

2. Theory

For emitting–absorbing media, the RTE can be written as

$$i(s) = \int_0^\infty i_\nu(0)\tau_\nu(0\rightarrow s)\,\mathrm{d}\nu + \int_0^\infty \int_0^s i_{\mathrm{b},\nu}(s')\frac{\delta\tau_\nu(s'\rightarrow s)}{\delta s'}\,\mathrm{d}s'\,\mathrm{d}\nu \quad (1)$$

where the transmissivity across a path from s to s' is defined by

$$\tau_\nu(s'\rightarrow s) = \exp\left(-\int_{s'}^{s} k_\nu(s'')\,\mathrm{d}s''\right) \quad (2)$$

For a grey, homogeneous medium, Eq. (2) simplifies to a recurrence relation expressing the intensity at the end of a path in terms of that at the start

$$i_n = i_{n-1}\tau_N + i_{\mathrm{b},N}(1-\tau_N) \quad (3)$$

The total transmissivity, τ_N, and the black body intensity, $i_{\mathrm{b},N}$, are assumed constant for the Nth control volume.

If Eq. (3) is expanded back to the origin of its path, the intensity at a point is expressed as

$$i_n = i_0\prod_{r=1}^{n}\tau_r + \sum_{r=1}^{n} i_{\mathrm{b},r}\epsilon_r \prod_{r'=r+1}^{n}\tau_{r'} \quad (4)$$

Eq. (4) represents a constant absorption coefficient (CAC) solution to the RTE such that, for constant values of k, the transmissivity is given by $\tau_r = \exp(-kl) = (1-\epsilon_r)$. As a new cell in a path is traversed, the transmissivity product for each upstream cell is multiplied by the transmissivity of the new cell. Whilst this approach is attractive computationally, it fails to address the multi-dimensional dependence of radiative exchange on local properties, on the history along a line-of-sight, and on the non-grey character of thermal radiation. Other than under uniform conditions, the use of a constant absorption coefficient throughout a domain can generate unacceptable errors particularly if the most appropriate value is not employed. Often, a reasoned 'guess' has to be made. It is also possible to use a number of absorption coefficients on a zone basis [19].

Table 1
Absorption and weighting coefficients for the weighted sum of grey gases model due to Truelove [20]—partial pressure ratio of CO_2–H_2O equal to 0.5. In Eq. (5), $a_{nn'}(T) = b_1 + b_2 T$

n	n'	b_1	$b_2 \times 10^3$	$k_{g,n}$ (m^{-1} atm^{-1})	$k_{p,n'}$ (m^{-4} kg^{-1})
1	1	0.588	−0.2401	0.0	541
1	2	−0.165	0.2834	0.0	2749
2	1	0.412	−0.1665	0.89	541
2	2	−0.127	0.2178	0.89	2749
3	1	0.2375	−0.0941	15.5	541
3	2	−0.0105	0.0265	15.5	2749
4	1	0.0585	−0.0243	239.0	541
4	2	0.0065	−0.0027	239.0	2749

2.1. Total property solution

The total property solution to the RTE represents an improvement over the CAC solution in that it includes the dependence of thermal radiation on local properties. Thus, it applies Eq. (4) with values of transmissivity and emissivity evaluated for each element in a path. Any radiative property model can be used. In the comparisons presented below, both the weighted sum of grey gases model and the narrow band model are employed. WSGG coefficients from [20] are used to evaluate total emissivities

$$\epsilon^{\mathrm{T}} = \sum_{n,n'} a_{n,n'}(T)\{1 - \exp[-k_{\mathrm{g},n}[p_{\mathrm{h}} + p_{\mathrm{c}}] - k_{\mathrm{p},n'}\rho_{\mathrm{p}}\Phi]L\} \quad (5)$$

which incorporates eight components. Values for these coefficients are tabulated in Table 1 for a partial pressure ratio of CO_2–H_2O equal to 0.5. The subscripts n and n' signify individual soot and gaseous components, and the temperature polynomial coefficients are such that Eq. (5) reduces to the soot free and soot dominant limits. Henceforth, each pair of these values is represented by a single value. Other sets of coefficients are available in [3] and [21].

When using the narrow band model, total emissivity is evaluated from

$$\epsilon^{\mathrm{T}} = 1 - \tau^{\mathrm{T}} = 1 - \int_0^\infty i_{\mathrm{b}}(T,\nu)\bar{\tau}_{\Delta\nu}\,\mathrm{d}\nu \Big/ \int_0^\infty i_{\mathrm{b}}(T,\nu)\,\mathrm{d}\nu \qquad (6)$$

where, for a single homogeneous element, the band transmissivity is given by the product of transmissivities of all contributing species [17].

2.2. The weighted sum of grey gases solution

Whilst the TP solution incorporates the dependence of radiative properties on temperature and composition, it ignores the non-grey character of emission and subsequent absorption. In contrast, the WSGG solution models all of these dependencies by solving separate transfer equations for the distinct grey components, each one of which comprises a group of relatively wide bands [22].

Thus, although the weighted sum of grey gases property model was originally devised to simply represent the total emissivity of combustion gases, it can also be applied in a line-of-sight solution to the RTE if Eq. (4) is solved for each grey gas, with the black body intensity pre-multiplied by the corresponding weighting coefficients [3]. So, for the jth grey gas

$$i_{j,n} = i_{0,j}\prod_{r=1}^{n}\tau_{j,r} + \sum_{r=1}^{n}\left[a_j i_{\mathrm{b},r}\epsilon_{j,r}\prod_{r'=r+1}^{n}\tau_{j,r'}\right] \qquad (7)$$

where transmissivities, $\tau_{j,r}$, emissivities, $\epsilon_{j,r}$, and the black body intensity, $i_{\mathrm{b},r}$, are evaluated using mean properties across individual elements, assumed constant for each element. The total intensity, i_n, is then a summation of that contributed by each grey gas. For black boundaries, the emitted radiation, $i_{0,j}$, is given by the black body intensity multiplied by the a_j coefficient, both evaluated at the boundary temperature. Eq. (7) has been applied to measured line-of-sight profiles of temperature, gas and soot concentrations in a furnace [23]. Predictions from the WSGG solution closely matched the radiative intensity measured by a narrow-angle probe, progressively withdrawn through the flame, and sighted on a target having a known leaving intensity. Such line-of-sight calculations are useful for assessing the accuracy of different algorithms in preparation for their use in a global radiation model.

In the DTRM, radiative energy exchange is evaluated by solving the RTE along individual lines-of-sight between boundary surface elements, and summing the contributions from the associated rays to surface and volumetric fluxes [2]. With black boundaries, it is a fairly straightforward procedure to apply Eq. (7) along each ray, since the initial intensity does not include any reflected radiation. However, when boundaries are grey, separate expressions are required for the incident radiation of each grey gas, so that the reflected fraction in the individual transfer equations results solely from irradiation due to the same component. Therefore, at every surface, for each grey gas, the incident intensity must be summed across all impinging rays. Thus, the initial intensity of the jth grey gas is

$$i_{0,j} = \left[a_j(T_0)\epsilon_0\sigma T_0^4 + [1-\epsilon_0]\sum_{m=1}^{M} w_m i_{m,j}\right]/\pi \qquad (8)$$

where the summation represents the total incident flux for the jth gas. The weighting coefficients, w_m, derive from the method of spatial discretisation [24].

2.3. The differential banded transmissivity (DBT) solution

When Eq. (4) is written for a particular wave number, the spectrally correlated intensity across a bandwidth $\Delta\nu$ is

$$i_\nu^{\mathrm{c}} = \frac{1}{\Delta\nu}\int_{\nu-(\Delta\nu/2)}^{\nu+(\Delta\nu/2)}\left\{i_\nu(0)\prod_{r=1}^{n}\tau_{\nu,r} + \sum_{r=1}^{n}\left[i_{\mathrm{b},\nu,r}\epsilon_{\nu,r}\prod_{r'=r+1}^{n}\tau_{\nu,r'}\right]\right\}\mathrm{d}\nu \qquad (9)$$

The correlation between emission and absorption is such that the history of every line emission must be traced. Downstream volumes in a path may or may not absorb energy from particular lines, and further emission may overlap other lines completely, partially or not at all. Clearly, the high resolution structure of the spectrum prohibits a complete representation of the correlation between intensity and absorptivity for engineering calculations. However, poor performance has been demonstrated [25] for a non-correlated solution

$$i_n = \sum_{j=1}^{J}\left[i_{0,j}\prod_{r=1}^{n}\bar{\tau}_{j,r} + \sum_{r=1}^{n}\left[\bar{i}_{\mathrm{b},j,r}\bar{\epsilon}_{j,r}\prod_{r'=r+1}^{n}\bar{\tau}_{j,r'}\right]\Delta\nu\right] \qquad (10)$$

where the strength, shape and distribution of individual lines was modelled by band descriptions of the spectrum, and mean values of intensity and transmissivity were used for each band.

The previous two algorithms focus on the recurrence interpretation of the RTE. If, however, the differential transmissivity in Eq. (1) is expanded, for each spectral band, as a finite difference at all upstream locations, the intensity becomes

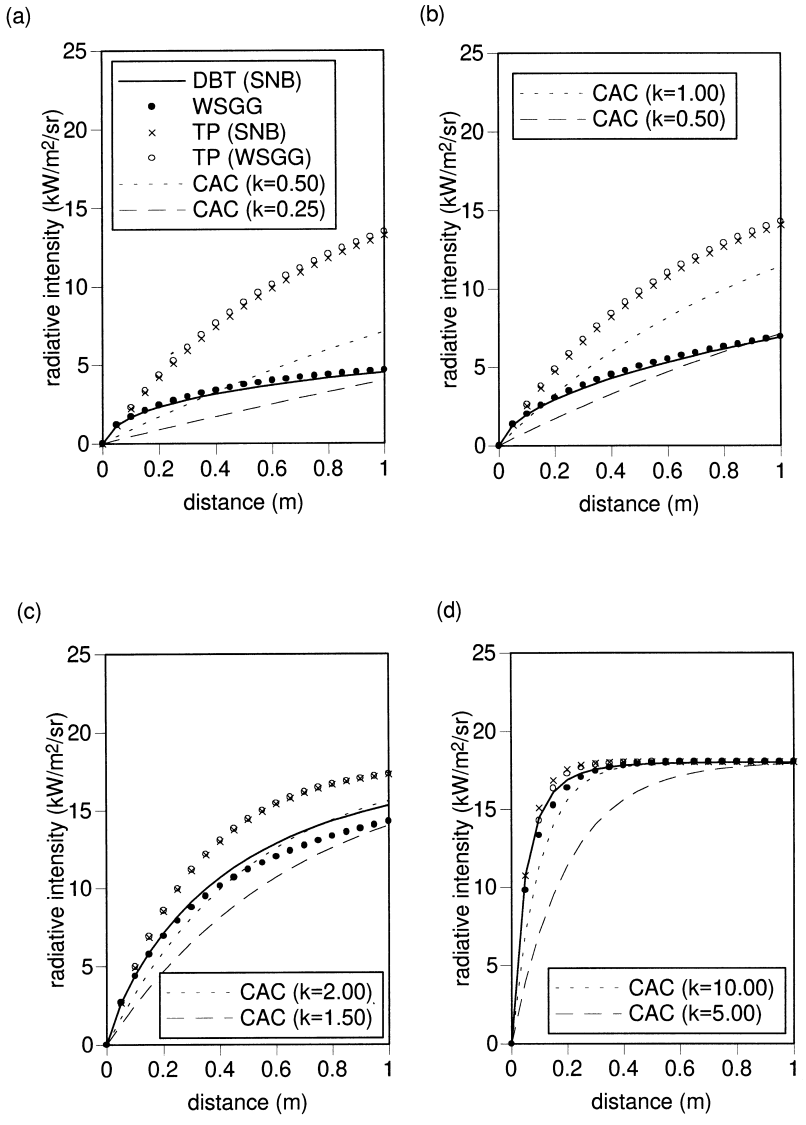

Fig. 1. Line-of-sight comparison between the WSGG and TP solutions to the RTE across a uniform CO_2–H_2O layer for various soot loadings: (a) $\Phi = 0.0$; (b) $\Phi = 1.0e{-}7$; (c) $1.0e{-}6$; (d) $1.0e{-}5$.

$$i_n = \sum_{j=1}^{J}\left[i_{0,j}\bar{\tau}_{0\to n,j} + \sum_{r=1}^{n} \bar{i}_b(T_s,\nu_j)[\bar{\tau}_{r\to n,j} - \bar{\tau}_{r-1\to n,j}]\Delta\nu_j \right] \tag{11}$$

For combustion gases, it has been shown that division of the spectrum into 5–25 cm^{-1} wave number intervals can facilitate the use of narrow band data in banded solutions to the RTE [17]. Thus, mean band transmissivities are evaluated from a narrow band gas property model. The transmissivity difference across an upstream cell is evaluated across paths from the leading and trailing edges of that cell. In Eq. (11), $\phi_{a\to b}$ denotes the value of a property, ϕ, across a path where a and b signify the initial and final points in the path, respectively. The spectral black body intensity

$$\bar{i}_b(T_s,\nu_j) = \frac{2C_1\nu_j^5}{e^{C_2\nu_j/T_s} - 1} \tag{12}$$

is evaluated at the centre of a band and midway between each path origin. C_1 and C_2 represent Planck's first and second constants, respectively.

Non-uniformities are normally treated by scaling the band parameters used to calculate the transmissivity.

When bands comprise more than one species, the transmissivity is calculated as the product of the individual species transmissivities. Eq. (11) represents the differential banded transmissivity solution to the RTE.

The initial intensity, $i_{0,j}$, is modelled in a similar way to that for the WSGG solution. For the jth band it is

$$i_{0,j} = \epsilon_0 \bar{i}_{\mathrm{b}}(T_0,\nu_j)\Delta\nu_j + \frac{[1-\epsilon_0]}{\pi}\sum_{m=1}^{M} w_m i_{m,j} \tag{13}$$

where the summation represents the total incident radiation within the band for all rays. Since solid wall radiation is treated as grey, account must be taken of the wings of the spectrum outside which the medium radiation is assumed to be negligible. This is accomplished by treating the wings as a separate band and applying Eq. (13) with the first term replaced by

$$\epsilon_0\left[\frac{\sigma T_0^4}{\pi} - \sum_{j=1}^{J}\bar{i}_{\mathrm{b}}(T_0,\nu_j)\Delta\nu_j\right] \tag{14}$$

3. Analysis

The following analysis principally compares the WSGG and TP solutions to the RTE relative to the differential banded transmissivity solution employing the statistical narrow band (SNB) model described above. Additional information is provided by appropriate constant absorption coefficient solutions. Initially, comparisons are made for single line-of-sight calculations across uniform and non-uniform mixtures. The non-uniform configurations are then analysed in a full DTRM calculation between solid walls.

3.1. Radiative intensity variation across uniform mixtures

The variation of radiative intensity across a selection of gas–soot mixtures is depicted in Fig. 1. In all cases,

$$T = 1000\ \mathrm{K};\quad p_{\mathrm{h}} = 2p_{\mathrm{c}} = 0.16;\quad L = 1.0\ \mathrm{m}$$

and the soot volume fraction takes the values 0.0; 1.0e−7; 1.0e−6; 1.0e−5. The CAC solutions are included to demonstrate the increasingly grey character of the other solutions produced by raising the soot concentration. In the absence of soot, no absorption coefficient produces a satisfactory representation of gaseous radiation.

The TP solutions performed using weighted sums of grey gases and narrow band property models agree very closely with each other. However, both of them produce increasing differences (with reduced soot loading) relative to the banded and grey gas component solutions.

Application of the TP solution to uniform paths generates equal cell-based absorption coefficients, and is therefore akin to a CAC solution, but with the absorption coefficient evaluated from local properties. Hence, radiation is treated as grey. The corresponding absorption coefficients for the TP solutions are approximately 1.4, 1.6, 3.2 and 15.7. However, molecular gases are non-grey, due to the distribution of absorption and emission lines of widely varying strengths and shapes which produce preferential self-absorption across the spectrum. Consequently, overall absorption across a path is likely to be under-estimated, as high absorptivity in particular regions of the spectrum is averaged across the whole spectrum. This characteristic can be demonstrated by considering the emitted intensity along a line-of-sight across a uniform path for two arbitrary bands (a and b) having different strengths (e_a, e_b) and transmissivities (τ_a, τ_b). The intensity across two equal path lengths evaluated by separate treatment of each band is given by

$$i_{\mathrm{banded}} = [e_a(1-\tau_a^2) + e_b(1-\tau_b^2)] \tag{15}$$

If, instead, a total transmissivity is defined as

$$\tau^{\mathrm{T}} = (\tau_a e_a + \tau_b e_b)/(e_a + e_b) \tag{16}$$

the intensity becomes

$$i_{\mathrm{total}} = (e_a + e_b)(1-(\tau^{\mathrm{T}})^2) \tag{17}$$

Simple algebraic manipulation then leads to

$$i_{\mathrm{total}} - i_{\mathrm{banded}} = e_a e_b(\tau_a - \tau_b)^2/(e_a + e_b) \tag{18}$$

such that $i_{\mathrm{total}} \geqslant i_{\mathrm{banded}}$. Thus, unless $\tau_a = \tau_b$, the use of total properties over-predicts intensity for the two bands emitting (and absorbing) across two identical path lengths. The same conclusion naturally follows for the entire spectrum since the same reasoning can be applied to an ensemble of band pairs. Despite this indictment of the total property solution, it has been commonly employed in the DTRM with total properties evaluated from the weighted sum of the grey gases property model [14].

Although the TP solution is essentially flawed, Fig. 1 demonstrates that its accuracy improves as the soot loading in gas–soot mixtures is increased. Experiments have demonstrated [26] that the single grey gas approximation becomes an increasingly good approximation of soot radiation as soot concentrates increases, thus validating the TP solution when gas radiation is dominated by that from soot.

The features just described are now investigated for non-uniform mixtures possessing property variations

Table 2
Temperature–partial pressure configurations. $L=1.0$

Configuration	Temperature (K)	Partial pressure of CO_2 (atm)
A	$4000s(L-s)+800$	$0.4s(L-s)+0.06$
B	$4000s(s-L)+1800$	$0.4s(s-L)+0.16$

characteristic of flames. These configurations are summarised in Tables 2 and 3.

3.2. Radiative intensity variation across non-uniform mixtures

In Fig. 2(a), the variation of radiative intensity is shown across a 1 m line-of-sight through a CO_2–H_2O mixture represented by configuration A (Table 2). Negligible differences occur between the WSGG and DBT solutions, both increasing through a point of inflection to a maximum close to the end of the line-of-sight. The decrease in intensity results from an increase in absorption over emission in the cooler, less dense outer edges of the path. Absorption coefficients of 0.25 and 0.75 bracket these solutions, but no value in this range satisfactorily captures the full shape of the profiles. The TP solutions, represented by an absorption coefficient just greater than 1.0, exhibit the same overall profile variation, but over-predict intensity by over 100% at locations beyond the mid-point of the line-of-sight.

The influence of soot is investigated by adding two concentration variations to configuration A. Generally, when the soot loading imposed on a gas mixture is increased, the overall radiative behaviour is dominated by the increasingly grey characteristics of soot. This is confirmed in Fig. 2(b) which shows the effect of a relatively heavy loading given by configuration As, $\Phi=[40s[1.0-s]+6]\times10^{-7}$, comprising a maximum of $\Phi=1.6\times10^{-6}$ on the centre line. Now, the TP solution agrees very closely with the DBT and WSGG solutions. An absorption coefficient of 5.0 in the CAC solution accurately represents all predictions. Due to the high soot concentration at the centre of the path, the intensity increases rapidly to a maximum which is

Table 3
Soot volume fraction configurations. $L=1.0$

Configuration	Soot volume fraction
As	$[40s(L-s)+6]\times10^{-7}$
Bs	$[40s(L-s)+6]\times10^{-8}$
Cs	$[4s(s-L)+1.6]\times10^{-6}$
Ds	$[4s(s-L)+1.6]\times10^{-7}$

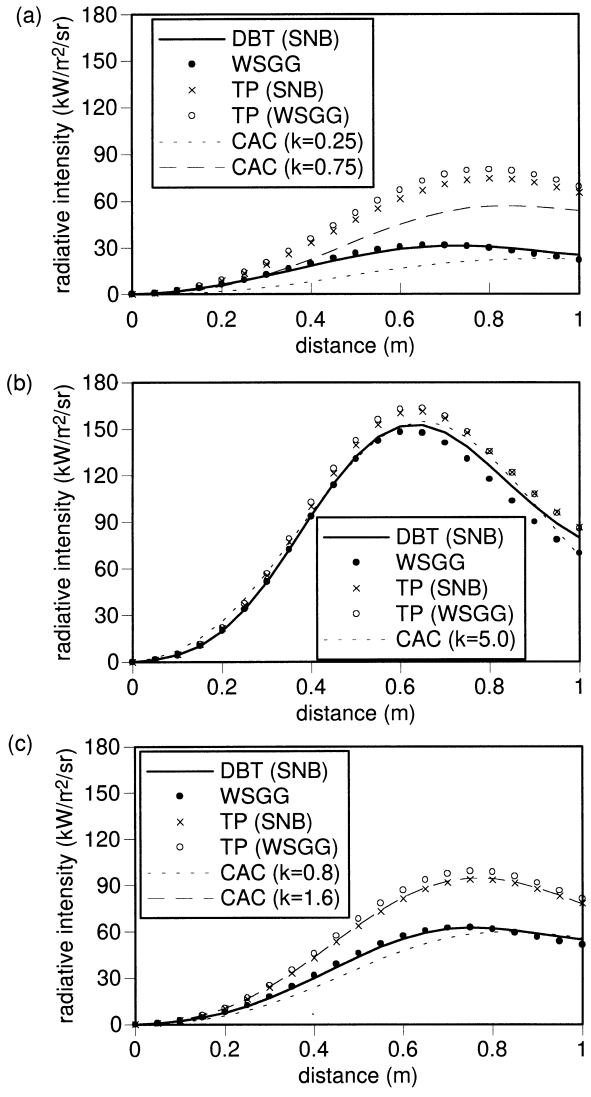

Fig. 2. Comparison between the WSGG and TP solutions to the RTE for configuration A across a CO_2–H_2O layer for various soot loadings: (a) no soot; (b) configuration As (high concentrations); (c) configuration Bs (intermediate concentrations).

almost five times greater than in Fig. 2(a). Additionally, the turning point is located closer to the centre line. Subsequently, the cooler, less dense outer edges exhibit considerable absorption as the intensity decreases to almost half of its peak value.

Since a low soot loading applied to configuration A has a minimal effect on the results (and associated conclusions) shown in Fig. 2(a), the other soot concentration variation considered here is representative of an intermediate range of soot loading. Under a variety of uniform conditions, an appropriate range has been identified to be approximately centred at a value of

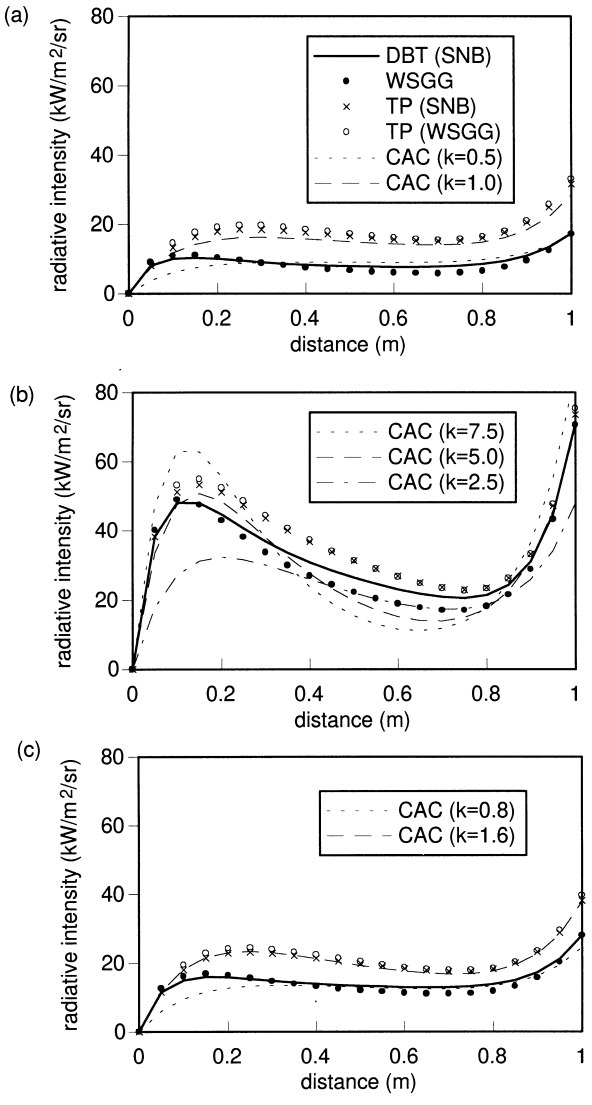

Fig. 3. Comparison between the WSGG and TP solutions to the RTE for configuration B across a CO_2–H_2O layer for various soot loadings: (a) no soot; (b) configuration Cs (high concentrations); (c) configuration Ds (intermediate concentrations).

$\Phi L = 10^{-7}$ m [27]. In order to encompass this range in the present analysis, a soot concentration variation is adopted given by configuration Bs, $\Phi = [40s[1.0-s]+6] \times 10^{-8}$ possessing a maximum centre line value of $\Phi = 1.6 \times 10^{-7}$. The intensity variation across configuration A combined with this intermediate soot loading is shown in Fig. 2(c). Relative to the intensity variation depicted in Fig. 2(a), the gradient of the profile either side of the inflection point is increased, and the final value of radiance is approximately double that shown for the gas mixture without soot. Although the presence of soot reduces errors produced by the TP solutions relative to the case of zero soot loading, significant errors (greater than 30%) are still evident. The TP solutions are represented by an absorption coefficient of 1.6, whilst a value of approximately 0.8 defines the DBT solution reasonably well.

The foregoing configurations are characteristic of non-premixed diffusion flames produced by an inner fuel core inflow, surrounded by an outer oxidant stream. A very different set of profiles characterise flames propagated by a core oxidant stream and a concentric fuel stream. Under these conditions, radial profiles of temperature and concentration increase from a minimum on the centre line to a maximum in the fuel stream. A simplified representation of this system is given by configuration B for temperature and the partial pressures of CO_2 and H_2O (Table 2). The line-of-sight radiative intensity variation across this configuration is shown in Fig. 3(a). Since the coolest temperature and lowest gaseous concentrations are located at the centre of the path, the initial hot, high density region produces high emission, but a point is quickly reached whereby the cooler, less dense region absorbs more than it emits. Thereafter, absorption and emission are effectively balanced until increasing density and temperature at the far end of the path culminate in further augmentation of the radiative intensity.

Figs. 3(b) and (c) show the effect of adding heavy and intermediate soot loadings to the gas mixture. These are given by configuration Cs, $\Phi = [4s[s-1.0] + 1.6] \times 10^{-6}$, and Ds, $\Phi = [4s[s-1.0] + 1.6] \times 10^{-7}$, respectively. In Fig. 3(b), the characteristic shape of Fig. 3(a) is significantly accentuated by the rapid increases in emission at the edges of the line-of-sight, and by a clearly defined central region of net absorption. An intermediate soot loading has a less marked effect on the profile as shown in Fig. 3(c).

For all three mixtures, the WSGG solution accurately predicts the DBT solution, and the TP solutions over-predict net emission in similar proportions to those observed for configuration A. Although each mixture appears to be defined by similar absorption coefficients to the ones used in the previous analysis, the heavy soot loading intensity variation could not be captured to the same level of accuracy. An absorption coefficient of 5.0 defines the initial maximum intensity, but then significantly under-predicts net absorption. In contrast, an absorption coefficient of approximately 2.5 greatly under-predicts intensity at the start of the path, but better predicts the minimum turning point.

Having demonstrated considerably different predictions by the WSGG and TP solutions applied to individual lines-of-sight, it is now necessary to assess their performance in a full DTRM calculation. For this purpose, the same mixtures are analysed bounded by infinite parallel walls. In all cases, the boundaries are

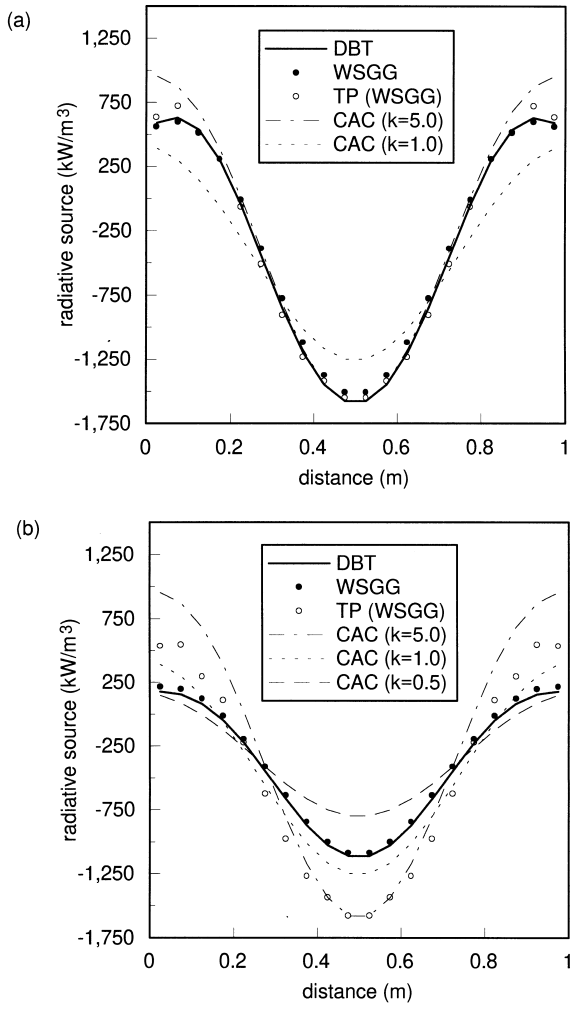

Fig. 4. Comparison of the WSGG and TP solutions for the prediction of volumetric flux variation across CO_2–H_2O–soot mixtures between cold black walls (configuration A): (a) heavy soot loading (configuration As); (b) intermediate soot loading (configuration Bs).

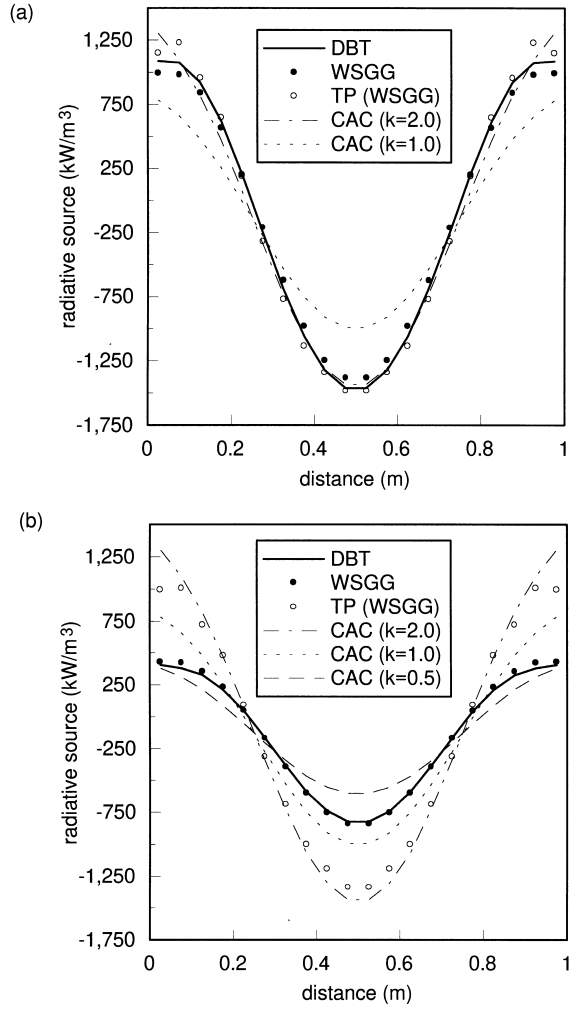

Fig. 5. Comparison of the WSGG and TP solutions for the prediction of volumetric flux variation across CO_2–H_2O–soot mixtures between cold low emissivity walls, $\epsilon = 0.25$ (configuration A): (a) heavy soot loading (configuration As); (b) intermediate soot loading (configuration Bs).

isothermal at the same temperature as the extremities of the mixture. Heavy and intermediate soot loadings are combined with configurations A and B, in predictions of the volumetric radiative flux between both black and low emissivity ($\epsilon = 0.25$) walls. The layer is divided into 20 elements, and 16 rays are launched from each wall. Differences of less than 1% were produced by increasing the grid and/or the ray number resolution.

3.3. DTRM calculation between cold walls

For configuration A with walls at 800 K, the hot mixture is a net emitter of radiation. The relatively cool edges, however, absorb a proportion of this energy before it arrives at the walls. This energy exchange yields the radiative source variation shown in Figs. 4 and 5. For $\epsilon = 1.0$, all of the mixture radiance is absorbed by the walls. When the walls have low emissivity, there is greater absorption by the mixture since a large fraction of radiation from the hot region is reflected at the walls. Consequently, higher wall reflectivity reduces the net emission from the mixture.

The radiative source variations between black boundaries are shown for heavy and intermediate soot loadings in Figs. 4(a) and (b), respectively. Relative to the intermediate soot loading, greater net emission from the high soot concentration produces increased

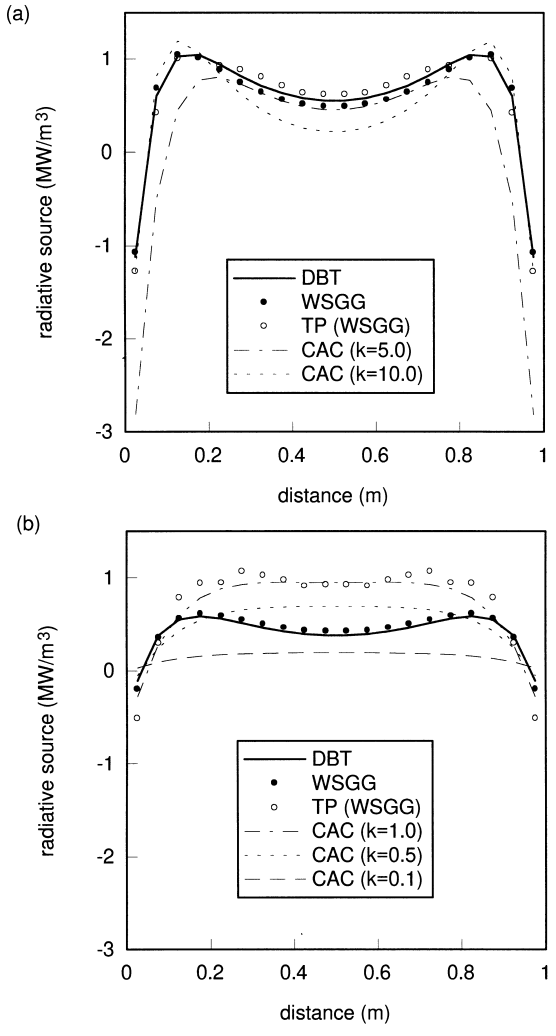

Fig. 6. Comparison of the WSGG and TP solutions for the prediction of volumetric flux variation across CO_2–H_2O–soot mixtures between hot black walls (configuration B): (a) heavy soot loading (configuration Cs); (b) intermediate soot loading (configuration Ds).

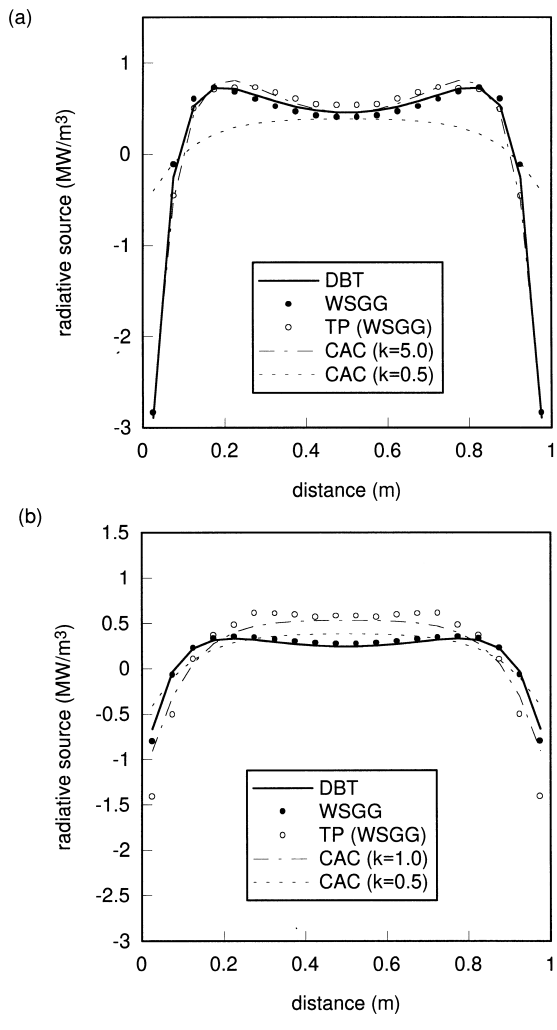

Fig. 7. Comparison of the WSGG and TP solutions for the prediction of volumetric flux variation across CO_2–H_2O–soot mixtures between hot low emissivity walls, $\epsilon = 0.25$ (configuration B): (a) heavy soot loading (configuration Cs); (b) intermediate soot loading (configuration Ds).

net absorption at the edges. A similar effect is produced by the TP simulation shown in Fig. 4(b), since the over-prediction of emission either side of the centre line leads to an over-prediction of net absorption in the cooler, less dense regions. Under heavy soot loading, this failing of the TP solution is almost indiscernible. The source term variation in Fig. 4(a) is accurately modelled by the TP solution. Close agreement is also produced for most of the layer by a CAC solution with an absorption coefficient equal to 5.0.

Similar characteristics apply to the prediction of source term variation between low emissivity walls as shown in Fig. 5. However, in addition to an overall increase in net absorption by all solutions as explained above, the TP solutions generate slightly larger errors than the calculations performed for black boundaries.

3.4. DTRM calculation between hot walls

When configuration B is applied between walls at 1800 K the mixture becomes an overall absorber. The greatest net absorption occurs approximately one fifth of the distance from each wall, thus generating the M-shaped radiative source variation shown in Figs. 6 and 7. Since maximum net absorption does not occur in the coolest, least dense regions, this profile serves to emphasise the complex dependence of radiative beha-

viour on phenomena which compete to redistribute energy.

In the black wall case, only a narrow region of the mixture adjacent to the walls emits more radiation than it absorbs. This region expands for the mixture between grey walls, and the absolute value of this loss increases due to the low emissivity of the walls. In contrast to the near wall effects for configuration A, radiation from the walls is now dominated by the high temperature of the walls as opposed to reflection of high temperature radiation from within the mixture.

Heavy soot loadings shown in Figs. 6(a) and 7(a) produce greater net emission close to the boundaries than is produced by the intermediate loadings shown in Figs. 6(b) and 7(b). Therefore, a higher energy flux flows into the interior of the layer, which, being of a greater density, absorbs more strongly than when there is a lower concentration of soot.

As before, the total property solutions over-predict both emission (in hot dense regions), and absorption (in locations of relatively low concentration and temperature). For the intermediate soot loading, errors in excess of 100% are produced at most locations, but significant errors are only evident for the heavy loading in the regions of net emission close to the walls.

Errors in the prediction of volumetric radiative flux has important implications for the simulation of real engineering systems. First, the prediction of highly non-linear pollutant formation is such that small errors in flow field temperature—which is dependent on volumetric radiative flux—can produce large errors in the mechanisms used to describe these processes. Second, the radiative flux to boundary surfaces is determined by the volumetric radiative flux, but care must be taken when assimilating wall fluxes since a cancellation of errors can occur if over-prediction of emission in one region is balanced by over-prediction of absorption in another. This is the case in the total property solutions for intermediate soot loadings shown in Figs. 4–7. Thus, large errors in volumetric radiative flux may or may not be evident in the distribution of radiative flux at boundary surfaces.

4. Conclusions

This paper has assessed the influence of soot when employing weighted sum of grey gases data in solutions to the radiative transfer equation. Individual line-of-sight calculations and the line-of-sight formulation of the discrete transfer radiation model have demonstrated that, for a wide range of soot loadings, the TP approach, which solves a single RTE having evaluated absorption coefficients from local properties on a cell-by-cell basis, can produce unsatisfactory simulation of complex radiative behaviour. However, accuracy of the TP solution does improve with increasing soot loading. In contrast, a WSGG solution to the RTE, incorporating a summation of separate solutions for each grey gas, yields close agreement with a narrow band, differential banded solution, even for low concentrations of soot.

Whilst current levels of computing power still mitigate against performing differential banded solutions within a full computational simulation of combusting flow fields, they are now at a level to permit the use of the WSGG solution in the discrete transfer radiation model. Thus, although the TP solution is less computationally expensive than the WSGG solution, and the TP solution can yield good accuracy in regions of high soot concentration, the analysis presented above has demonstrated that it is considerably more accurate to use the weighted sum of grey gas data in the WSGG solution. Further work is required to reinforce these results when the different solution strategies are applied to experimentally validated combustion systems, and to assess the effect of radiative flux prediction on other modelled processes, especially pollutant formation.

References

[1] N.W. Bressloff, J.B. Moss, P.A. Rubini, CFD prediction of coupled radiation heat transfer and soot production in turbulent flames, in : Twenty-sixth International Symposium on Combustion. vol. 2, Combustion Institute, Pittsburg, PA, 1996, pp. 2379–2386.

[2] F.C. Lockwood, N.G. Shah, A new radiation solution method for incorporation in general combustion prediction procedures, in: Eighteenth International Symposium on Combustion, The Combustion Institute, Pittsburg, PA, 1981, pp. 1405–1414.

[3] M.F. Modest, The weighted-sum-of-gray-gases model for arbitrary solution methods in radiative transfer, J. Heat Transfer 113 (1991) 650–656.

[4] C.L. Tien, S.C. Lee, Flame radiation, Prog. Energy Combust. Sci. 8 (1982) 41–59.

[5] R. Viskanta, M.P. Menguc, Radiation heat transfer in combustion systems, Prog. Energy Combust. Sci. 13 (1987) 97–160.

[6] T.J. Kim, J.A. Menart, H.S. Lee, Nongray radiative gas analysis using the S–N discrete ordinates method, J. Heat Transfer 113 (1991) 946–952.

[7] T.H. Song, Comparison of engineering models of nongray behaviour of combustion products, Int. J. Heat Mass Transfer 36 (16) (1993) 3975–3982.

[8] J. Liu, S.N. Tiwari, Investigation of radiative transfer in nongray gases using a narrow band model and Monte Carlo simulation, J. Heat Transfer 116 (1994) 160–166.

[9] P. Docherty, M. Fairweather, Predictions of radiative transfer from nonhomogeneous combustion products using the discrete transfer method, Combust. Flame 71 (1988) 79–87.

[10] A. Soufiani, E. Djavdan, A comparison between weighted sum of gray gases and statistical narrow-band radiation models for combustion applications, Combust. Flame 97 (1994) 240–250.
[11] N.W. Bressloff, J.B. Moss, P.A. Rubini, Assessment of a differential total absorptivity solution to the radiative transfer equation as applied in the discrete transfer radiation model, Numerical Heat Transfer, Part B: Fundamentals 29 (3) (1996) 381–397.
[12] N.W. Bressloff, J.B. Moss, P.A. Rubini, Differential total absorptivity solution to the radiative transfer for mixtures of combustion gases and soot, Numerical Heat Transfer, Part B: Fundamentals 31 (1) (1997) 43–60.
[13] N.W. Bressloff CFD prediction of coupled radiation heat transfer and soot production in turbulent flames. PhD thesis, Cranfield University, UK 1996.
[14] F.C. Lockwood, W.M.G. Malalasekera, Flash over, in: Twenty-second International Symposium on Combustion, The Combustion Institute, Pittsburg, PA, 1988, pp. 1319–1328.
[15] D.F. Fletcher, J.H. Kent, V.B. Apte, A.R. Green, Numerical simulations of smoke movement from a pool fire in a ventilated tunnel, Fire Safety Journal 23 (1994) 305–325.
[16] M. Fairweather, W.P. Jones, R.P. Lindstedt, Predictions of radiative transfer from a turbulent reacting jet in a cross-wind, Combust. Flame 89 (1992) 45–63.
[17] W.L. Grosshandler, Radiative heat transfer in nonhomogeneous gases: a simplified approach, Int. J. Heat Mass Transfer 23 (1980) 1447–1459.
[18] C.B. Ludwig, W. Malkmus, J.E. Reardon, J.A.L. Thomson, Handbook of infrared radiation from combustion gases, NASA SP-3080, Scientific and Technical Information Office, Washington, DC, 1973.
[19] A. Haidekker, A. Charette, Y.S. Kocaefe, Application of the hybrid zone/Monte Carlo method to 3-D curvilinear grids in radiative heat transfer, Int. J. Num. Meth. Eng. 37 (1994) 203–216.
[20] J.S. Truelove, Zone method for radiative heat transfer calculations, HTFS DR33, AERE, Harwell, Oxon, UK, 1975.
[21] J.D. Felske, T.T. Charalampopolous, Gray gas weighting coefficients for arbitrary gas–soot mixtures, Int. J. Heat Mass Transmissivity 25 (12) (1982) 1849–1855.
[22] H.C. Hottel, A.F. Sarofim, Radiative Transfer, McGraw-Hill, New York, 1967.
[23] T.R. Johnson, J.M. Beer, J. Inst. Fuel 46 (1973) 301–309.
[24] N.W. Bressloff, J.B. Moss, P.A. Rubini, Application of a new weighting set for the discrete transfer radiation model, in: Proceedings of the 3rd European Conference on Industrial Furnaces and Boilers, Lisbon, Portugal, 1995.
[25] J. Taine, A line-by-line calculation of low-resolution radiative properties of CO_2–CO-transparent nonisothermal gas mixtures up to 3000 K, J. Quant. Spectroc. Radiat. Transfer 30 (4) (1983) 371–379.
[26] G.H. Markstein, Radiative energy transfer from gaseous diffusion flames, in: Fifteenth International Symposium on Combustion, The Combustion Institute, Pittsburgh, 1974, pp. 1285–1294.
[27] J.D. Felske, C.L. Tien, Calculation of the emissivity of luminous flames, Combust. Sci. Tech. 7 (1973) 25–31.